

Friends not Foes: Strong Correlation between Inner Super-Earths and Outer Gas Giants

MARTA L. BRYAN^{1, 2} AND EVE J. LEE^{3, 4}

¹David A. Dunlap Department of Astronomy & Astrophysics, University of Toronto, 50 St. George St., M5S 3H4 Toronto ON, Canada

²Department of Chemical & Physical Sciences, University of Toronto Mississauga, 3359 Mississauga Road, L5L 1C6 Mississauga ON, Canada

³Department of Physics and Trottier Space Institute, McGill University, 3600 rue University, H3A 2T8 Montréal QC, Canada

⁴Trottier Institute for Research on Exoplanets (*iREx*), Université de Montréal, Canada

ABSTRACT

The connection between outer gas giants and inner super-Earths reflects their formation and evolutionary histories. Past work exploring this link has suggested a tentative positive correlation between these two populations, but these studies have been limited by small sample sizes and in some cases sample biases. Here we take a new look at this connection with a sample of 184 super-Earth systems with publicly available radial velocity data and resolved outer gas giants. We calculate the frequency of outer gas giants (GG) in super-Earth (SE) systems, dividing our sample into metal-rich ($[Fe/H] > 0$) and metal-poor ($[Fe/H] \leq 0$) hosts. We find $P(GG|SE, [Fe/H]>0) = 28.0^{+4.9\%}_{-4.6\%}$ and $P(GG|SE, [Fe/H]\leq 0) = 4.5^{+2.6\%}_{-1.9\%}$. Comparing these conditional occurrence rates to field giant occurrence rates from Rosenthal et al. (2021), we show that there is a distinct positive correlation between inner super-Earths and outer gas giants for metal-rich host stars at the 2.7σ level, but this correlation disappears for metal-poor systems. We further find that, around metal-rich stars, the GG/SE correlation enhances slightly for systems with giants that are more distant (beyond 3 AU), more eccentric ($e > 0.2$), and/or in multi-gas giant systems. Such trends disappear around metal-poor stars with the exception of systems of multiple giants in which we observe a tentative anti-correlation. Our findings highlight the critical role metallicity (disk solid budget) plays in shaping the overall planetary architecture.

1. INTRODUCTION

Gas giants dominate the dynamics of the systems they are in and reflect earlier formation conditions. In our solar system, Jupiter and Saturn are believed to have played a dominant role in our system’s history, from opening gaps in the disk that could shape the surface density profile and composition of planetary building blocks in the inner system, to kicking volatile rich planetesimals onto shorter period orbits (e.g., Morbidelli et al. 2007; Walsh et al. 2011; Batygin & Laughlin 2015). We expect extrasolar gas giants to play a significant role in the lives of small planets as well.

The connection between inner super-Earths and outer gas giants was first explored in Zhu & Wu (2018) and Bryan et al. (2019). Both studies found that outer gas giants do not hinder the formation of super-Earths, and instead show a positive correlation between the two populations. In addition, most of the gas giant companions were found around metal-rich host stars, indicating metallicity is an important factor driving this correlation. Subsequent theoretical work explains this excess of cold Jupiters in super-Earth systems by showing that for systems with enough solids to produce a gas giant,

they naturally deliver enough material to the inner system for super-Earths to grow (e.g., Chachan et al. 2022; Chachan & Lee 2023) since most of the solids are lost to radial drift rather than being coagulated into planetary cores at large orbital distances (e.g., Lin et al. 2018).

While there have been follow-up efforts that also find a positive correlation between gas giants and small planets (e.g. Herman et al. 2019; Rosenthal et al. 2022), some have reported a neutral or even negative correlation (e.g. Bonomo et al. 2023). A resolution to this debate was presented in Zhu (2023), arguing that interpreting this correlation requires considering the host star metallicity distribution of the sample of systems. Namely, since the vast majority of the gas giants in all samples considered to date are found around metal-rich stars, having a sample of systems dominated by metal-poor stars (as was the case in Bonomo et al. (2023)) can bias the strength of the correlation. Zhu (2023) showed that when only considering the metal-rich systems in Zhu & Wu (2018), Bryan et al. (2019), and Bonomo et al. (2023), all three find consistent positive correlations between super-Earths and cold gas giants.

Three key takeaways from this debate are: 1) all studies to date have worked with small sample sizes, which makes interpreting the inner-outer planet correlation with statistical significance challenging; 2) properly accounting for sample biases in metallicity is a critical component of this interpretation; and 3) when sample biases are addressed, previous studies find consistent tentative positive correlations between inner super-Earths and outer gas giants.

In this paper, we explore the connection between inner super-Earths and outer gas giants with a sample of 184 systems, at least three times larger than previous samples considered, with the orbit of giant(s) resolved by radial velocity data. In Section 2, we describe how these systems were selected. Section 3 details our computation of sensitivity maps and completeness correction for each system, and Section 4 shows how we incorporate those maps into our occurrence rate calculations to compute the frequency of cold gas giants in super-Earth systems that are metal rich $P(\text{GG}|\text{SE}, [\text{Fe}/\text{H}] > 0)$ and metal poor $P(\text{GG}|\text{SE}, [\text{Fe}/\text{H}] \leq 0)$. To assess the presence and strength of a correlation, we compare our conditional probabilities to gas giant occurrence rates $P(\text{GG}|[\text{Fe}/\text{H}] > 0)$ and $P(\text{GG}|[\text{Fe}/\text{H}] \leq 0)$ from Wittenmyer et al. (2020) (hereafter denoted W20) and from Rosenthal et al. (2021) (hereafter denoted R21) in Section 5. Section 6 explores how gas giant properties shape this correlation, and Section 7 summarizes our findings, placing them in the context of formation theory.

2. OBSERVATIONS

We select systems with the following five criteria: the system has 1) publicly available radial velocity (RV) datasets, 2) at least one confirmed super-Earth planet ($1-20 M_{\oplus}$; $1-4 R_{\oplus}$), 3) host star mass greater than $0.6 M_{\odot}$ to exclude M-dwarfs, 4) RV datasets with baselines greater than one year and more than 20 data points, and 5) an RV semi-amplitude $K > 1 \text{ m/s}$ in the case of systems with super-Earths discovered using RVs to minimize the inclusion of false positive planets. We exclude M-dwarfs from this analysis for several reasons. Given the selection criteria above, there are 78 systems with host star masses $< 0.6 M_{\odot}$ that we could consider. However, out of the 203 stars in W20, only 8 are M-dwarfs. While the fraction of the R21 sample that are M stars is higher (121 M-dwarfs out of 719 stars), given the relevance of the W20 sample to this study we leave the assessment of the gas giant/super-Earth correlation around M-dwarfs to subsequent work. We additionally exclude a handful of systems that do not have published metallicity measurements. This yields a total of 184 systems (see Table

A.1). 109 of these systems have one or more super-Earth initially discovered via the transit method (hereafter labeled ‘transit sample’), and 75 systems have one or more super-Earth initially discovered with RVs (labeled ‘RV sample’). As described in the following section, we initially consider these samples separately due to the significant average difference in sensitivities to distant gas giants.

Of the systems in the transit sample, 56 are metal-rich $[\text{Fe}/\text{H}] > 0$, and 53 are metal-poor $[\text{Fe}/\text{H}] \leq 0$. Similarly, the RV sample has 39 metal-rich systems and 36 metal-poor ones. We consider a system to host a gas giant ($0.5-20 M_{\text{Jup}}$) if there is a confirmed gas giant (typically with $\gtrsim 1$ measured RV orbit) in the system. Given this criteria, there are 19 systems in the transit sample hosting at least one gas giant, 17 of which are metal-rich. The RV sample has 11 systems with one or more gas giants, 10 of which are metal rich. Properties of the gas giants in this sample are shown in Table A.2. We show host star properties of our sample in Figure 1.

3. SAMPLE SENSITIVITY MAPS

With a heterogeneous sample such as that considered here, individual system sensitivities to outer gas giants can vary widely due to differences in time baseline, observing cadence, number of data points, and measurement precision. For each system, we quantify sensitivity by calculating completeness as a function of mass and semi-major axis given the system’s RV dataset (see Table A.1 for references).¹ We start with a 50×50 grid in mass and semi-major axis evenly spaced in log space from $0.3-30 M_{\text{Jup}}$ and $0.3-30 \text{ AU}$. We inject 50 simulated planets into each grid box, each time drawing a mass and semi-major axis value from a uniform distribution across each grid box, an eccentricity from the β distribution, an inclination i from a uniform distribution in $\cos i$, and remaining orbital elements from uniform distributions.

We calculate simulated RVs at each observational epoch for the simulated planet, and add noise by drawing from a Gaussian distribution with a width defined by the instrumental uncertainty randomly shuffled from the original dataset. To determine whether a simulated planet would be detected, we fit each simulated RV series with a one-planet orbital solution and a flat line and compare the Bayesian information criterion (BIC) values from the two fits. A simulated planet is ‘detected’ if the one-planet model BIC is smaller than the flat line BIC

¹ In the case where there is more than one public RV dataset that has a time baseline > 1 year and more than 20 data points, we select the dataset that has higher completeness.

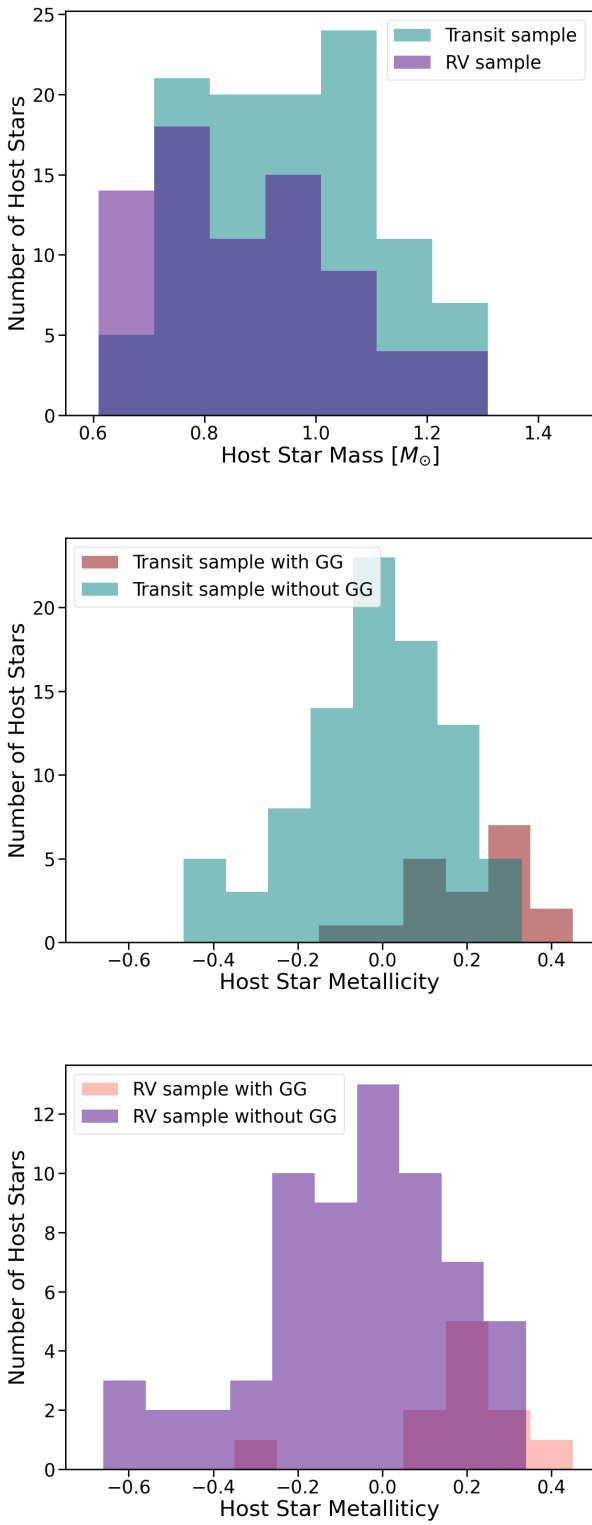


Figure 1. Top: Host star mass distributions for the transit super-Earth sample (teal) and the RV super-Earth sample (purple). Middle: Host star metallicity distributions for the transit super-Earth sample without gas giants (teal), and with gas giants (maroon). Bottom: Host star metallicity distributions for the RV super-Earth sample without gas giants (purple) and with gas giants (pink). Gas giants considered are $0.5-20 M_{Jup}$ and < 10 AU (see Table A.2 for properties).

by more than 10. In contrast, if the flat line is preferred or the one-planet model is preferred by a $\Delta BIC < 10$, the simulated planet is ‘not detected’. After repeating this process for each injected planet, we used our ‘detected’ vs ‘non-detected’ results to calculate completeness across the entire mass/semi-major axis grid.

Figure A.1 in the appendix presents average completeness maps for the RV super-Earth sample (top) and the transit super-Earth sample (bottom). Detected gas giants in each sample are overplotted. The reason why we initially separate these samples in our analysis is evident: on top of variations amongst individual systems, on average the RV sample systems have significantly higher sensitivities, driven by as much as an order of magnitude more data points and longer time baselines in comparison to the transit sample. Despite these differences, confirmed gas giants are in regions of parameter space where both transit and RV samples are on average close to, if not at, 100% completeness. This motivates our mass and semi-major axis ranges considered in our occurrence rate calculations in the following sections, namely $0.5-20 M_{Jup}$ and $1-10$ AU. Individual sensitivity maps allow us to account for completeness to gas giants in this range on a system-by-system basis in these calculations, and confirm that these sensitivity differences do not bias our results.

4. CONSISTENT OCCURRENCE RATES $P(GG|SE)$ FOR TRANSIT AND RV SAMPLES

To explore the connection between super-Earths and Jupiters, we start by calculating the frequency of gas giants (GG) in systems with inner super-Earths (SE), $P(GG|SE)$. We define these gas giants as planets with mass $0.5-20 M_{Jup}$ and orbital distance $1-10$ AU. Previous work has demonstrated the importance of host star metallicity to this GG/SE connection (Zhu 2023). We split our sample into metal-rich systems $[Fe/H] > 0$, and metal-poor systems $[Fe/H] \leq 0$ to verify the sensitivity of this correlation to metallicity.

We determine $P(GG|SE, [Fe/H] > 0)$ and $P(GG|SE, [Fe/H] \leq 0)$ using a general binomial distribution. If all of our systems had 100% completeness across our entire integration range ($0.5-20 M_{Jup}$ and $1-10$ AU), the posterior distribution given number of detections n_{det} and total number of systems n_{tot} is:

$$f(x; a, b) = \frac{1}{B(a, b)} x^{a-1} (1-x)^{b-1} \quad (1)$$

where B is the beta function, $a = n_{\text{det}} + 1$, and $b = n_{\text{tot}} - n_{\text{det}} + 1$. To correct for individual system sensitivities to gas giants, we used the completeness maps we computed for each system. We sum over the $0.5-20 M_{Jup}$ and

1–10 AU range and determine the average completeness for the set of systems considered. The coefficient b then becomes $b = (n_{\text{eff}} - n_{\text{det}}) + 1$, where n_{eff} is the total number of systems modified by the sample completeness.

We initially consider the RV and transit samples separately to test whether the average differences in system sensitivity impact the resulting occurrence rates. There are 56 metal-rich transit sample systems, 14 of which host one or more gas giants $0.5\text{--}20 M_{\text{Jup}}$ and 1–10 AU, 53 metal-poor transit sample systems with 2 hosting gas giants, 39 metal-rich RV sample systems with 10 hosting gas giants, and 36 metal-poor RV sample systems with just one hosting a gas giant. We find that the frequencies of gas giants in super-Earth systems for both metal poor and metal rich systems are consistent when comparing the RV and transit samples: $P(\text{GG|SE}, [\text{Fe}/\text{H}]>0) = 28.8 (+6.5\text{--}6.0)\%$ for the transiting sample and $P(\text{GG|SE}, [\text{Fe}/\text{H}]>0) = 27.8 (+7.5\text{--}6.8)\%$ for the RV sample, consistent to 0.1σ . Similarly, the metal poor RV and transit samples are consistent at the 0.1σ level, with $P(\text{GG|SE}, [\text{Fe}/\text{H}]\leq 0) = 5.5 (+3.9\text{--}2.7)\%$ for the transit sample and $P(\text{GG|SE}, [\text{Fe}/\text{H}]\leq 0) = 4.8 (+4.4\text{--}3.8)\%$ for the RV sample. We can therefore move forward with a combined RV+transit sample occurrence rate for the rest of the analyses. For this combined sample, we calculate conditional occurrence rate $P(\text{GG|SE}, [\text{Fe}/\text{H}]>0) = 28.0 (+4.9\text{--}4.6)\%$, and a substantially lower frequency for metal poor systems, $P(\text{GG|SE}, [\text{Fe}/\text{H}]\leq 0) = 4.5 (+2.6\text{--}1.9)\%$ (see Table 1).

5. A STRONG POSITIVE CORRELATION BETWEEN SE/GG FOR METAL RICH SYSTEMS

To assess whether there is a positive, negative, or no correlation between super-Earths and gas giants in our sample, we need to compare our conditional occurrence rate $P(\text{GG|SE})$ to the field occurrence of gas giants $P(\text{GG})$. For $P(\text{GG})$, we use the sample of systems from Rosenthal et al. (2021) (R21) and Wittenmyer et al. (2020) (W20). R21 presents the California Legacy Survey, a catalog of radial velocities for 719 stars observed over the course of 30 years. In this paper we take all systems in the R21 sample except M-star hosts ($<0.6 M_{\odot}$) and remaining systems with datasets < 20 RV measurements (4 systems). This yields 351 metal rich systems, 43 of which host gas giants ($0.5\text{--}20 M_{\text{Jup}}$ and 1–10 AU); and 243 metal-poor systems, 9 of which host gas giants (same definition as the metal-rich sample). Note again that we exclude M-dwarfs from this analysis to ensure consistent comparison. We leave the assessment of the GG/SE correlation around M-dwarfs to subsequent work. In this section we also consider the

W20 sample, which comes from the Anglo-Australian Planet Search that leverages the 18-year archive of data for 203 stars. Here we use all systems in the W20 sample except ones that are M-dwarfs and ones that do not have published stellar metallicities. The W20 sample considered here has 107 metal-rich stars, 14 of which host gas giants; and 87 metal-poor stars, 5 of which have one or more gas giants. Despite the smaller sample size, we initially include the W20 $P(\text{GG})$ value in our analysis since previous work examining the inner-outer planet correlation (e.g., Zhu 2023; Bonomo et al. 2023) used the W20 sample for $P(\text{GG})$ when interpreting their values for $P(\text{SE|GG})$.

To compare our value of $P(\text{GG|SE})$ to the R21 and W20 values for $P(\text{GG})$, it is critical to 1) use the same definition of a gas giant, namely mass and semi-major axis ranges considered, and 2) use comparable estimates for sensitivity corrections. For the R21 sample, we calculate individual system sensitivity maps for the whole sample using our methods outlined in Section 3 using the public radial velocities. Since RVs are not public for the W20 sample, we instead compare our sensitivity estimate methods. In short, W20 carries out injection/recovery simulations where they assess whether a planet has been “detected” based on whether a Lomb-Scargle periodogram can recover that signal with a false alarm probability (FAP) $< 1\%$ (see W20 for details). To test whether our method presented in Section 3 is comparable, we recalculate sensitivity maps for all of our systems using the W20 LS method. We find $P(\text{GG|SE}, [\text{Fe}/\text{H}]>0) = 26.3 (+4.6\text{--}4.4)\%$ and $P(\text{GG|SE}, [\text{Fe}/\text{H}]\leq 0) = 4.2 (+2.4\text{--}1.8)\%$, consistent with our original values to 0.3σ and 0.1σ respectively. We can thus move forward with our comparisons of $P(\text{GG})$ and $P(\text{GG|SE})$.

With consistent sensitivity corrections, we calculate $P(\text{GG}|[\text{Fe}/\text{H}]>0)$ and $P(\text{GG}|[\text{Fe}/\text{H}]\leq 0)$ for the R21 and W20 samples, using consistent definition of a gas giant ($0.5\text{--}20 M_{\text{Jup}}$ and 1–10 AU). Figure 2 and Table 1 show our results. For both metal rich and metal poor systems, the $P(\text{GG})$ frequencies from R21 and W20 are consistent to $<1\sigma$. From here we solely consider the R21 $P(\text{GG})$ occurrence rates throughout the rest of the paper due to the greater statistical leverage stemming from a significantly larger sample size in comparison to W20. For metal-rich systems, we find a distinct positive correlation between gas giants and super-Earths at the 2.7σ level. There are more gas giants in metal-rich super-Earth systems than you would expect just based on chance. In contrast, for metal poor systems the positive correlation disappears. These results highlight the importance of this metallicity dimension when interpret-

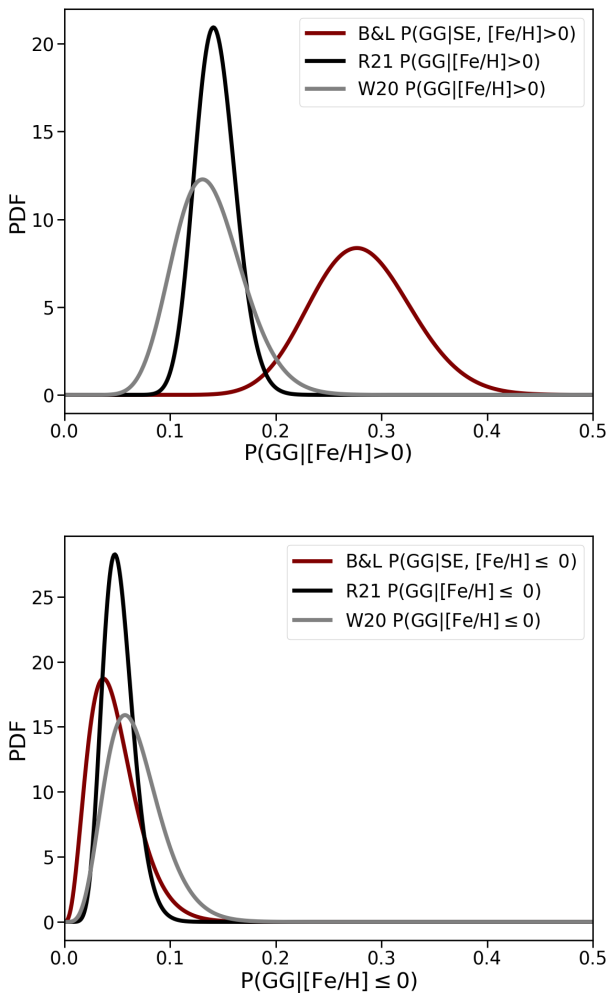


Figure 2. Top: Comparison of our conditional occurrence rate $P(\text{GG}|\text{SE})$ (maroon) to field giant occurrence rates $P(\text{GG})$ from the R21 sample (black) and the W20 sample (gray) for metal-rich stars. Bottom: The same comparison for metal poor systems. We see a positive correlation between super-Earths and gas giants for metal rich systems, namely $P(\text{GG}|\text{SE}, [\text{Fe}/\text{H}]>0) > P(\text{GG}|[\text{Fe}/\text{H}]>0)$ at the 2.7σ level, where $P(\text{GG})$ is taken from the larger R21 sample. This correlation disappears when moving to metal poor systems.

ing the SE/GG correlation. If a sample is biased towards low metallicities or there is a mixture of low and high, the strength of the correlation can be artificially underestimated.

Given the size of our sample and that of R21, we break both samples up into three metallicity bins to explore the dependence of the correlation on metallicity further: 1) $[\text{Fe}/\text{H}]<-0.1$; 2) $-0.1 \leq [\text{Fe}/\text{H}] \leq 0.1$; 3) $[\text{Fe}/\text{H}]<0.1$. Figure 3 shows that while there is no significant correlation between super-Earths and GG around stars in the first two bins, the most metal-rich bin has an even stronger

positive correlation between the two populations, at the 3.4σ level.

6. EFFECT OF GAS GIANT PROPERTIES ON THE CORRELATION

We now break up our sample into gas giant orbital distance, eccentricity, and multiplicity to determine the role the outer planet plays in shaping the architecture of planetary systems.

First we consider the impact of gas giant orbital distance on the SE/GG connection. We divide our systems into two samples, those with ‘close’ gas giants, and those with ‘distant’ gas giants. We experiment with four definitions of ‘close’ and ‘distant’: 1) 0.1-3AU and 3-10AU; 2) 0.1-2AU and 2-10AU; 3) 0.3-2AU and 2-10AU; and 4) 0.3-3AU and 3-10AU. This fourth definition matches that of Rosenthal et al. (2022), which explored the impact of gas giant location on the SE/GG correlation with a significantly smaller sample size of super-Earth systems. We divide the R21 sample in the same way. For each of these four distance combinations, we calculate the frequencies of closer and further gas giants as a function of metallicity. Note that for both our sample and R21 we treat multi-gas giant systems the same, counting systems twice if they have gas giants in both bins. For all four sets of semi-major axis ranges for ‘close’ and ‘distant’ gas giants, we find that the positive correlation between super-Earths and close gas giants around metal-rich stars $P(\text{GG}|\text{SE}, [\text{Fe}/\text{H}]>0) > P(\text{GG}|[\text{Fe}/\text{H}]>0)$ is slightly weaker than the positive correlation between super-Earths and distant gas giants by $0.2\text{--}0.4\sigma$, but still significantly positive. This runs counter to the tentative findings from Rosenthal et al. (2022) that suggest close gas giants suppress super-Earth formation in their small sample of 28 super-Earth systems. We additionally find that we see no significant SE/GG correlation around metal-poor hosts regardless of gas giant semi-major axis.

How might evidence of a dynamically hot or cold history imprint on the SE/GG connection? We divide our sample into systems that have high eccentricity gas giants ($e > 0.2$), and systems with gas giants that have low eccentricities ($e < 0.2$). For the eccentric gas giant case around metal-rich stars, we see a slightly stronger strength of the positive correlation, $P(\text{GG}|\text{SE}, [\text{Fe}/\text{H}]>0) = 20.1 (+4.5\text{--}4.0)\% > P(\text{GG}|[\text{Fe}/\text{H}]>0) = 7.1 (+1.5\text{--}1.3)\%$ at the 3.0σ level. However, for dynamically cold metal-rich systems this positive correlation substantially diminishes, dropping to a significance of 1.3σ (Table 1). True to form, metal-poor systems do

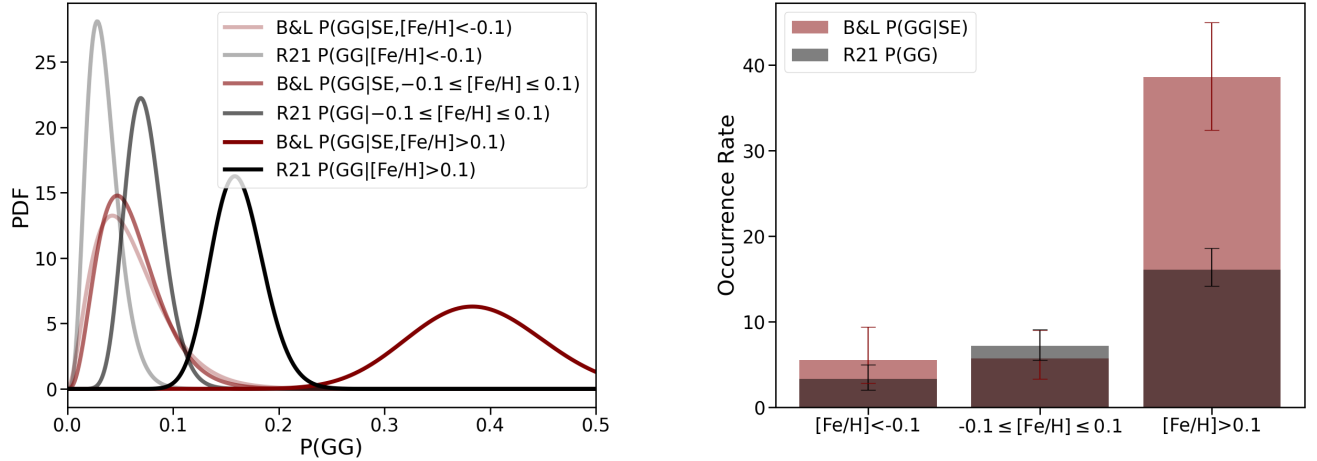


Figure 3. We compare our occurrence rate $P(\text{GG}|\text{SE})$ to that of R21 $P(\text{GG})$ for three metallicity ranges: 1) $[\text{Fe}/\text{H}] < -0.1$; 2) $-0.1 \leq [\text{Fe}/\text{H}] \leq 0.1$; 3) $[\text{Fe}/\text{H}] > 0.1$. Left panel shows the posterior distributions, right panel shows those distributions represented as histogram bins. While the $P(\text{GG}|\text{SE})$ and $P(\text{GG})$ occurrence rates are consistent to $<1\sigma$ for the low and medium metallicity bins, the high metallicity bin has a significantly higher frequency of gas giants in super-Earth systems, greater than $P(\text{GG})$ by 3.4σ . The positive correlation gets even stronger when host star metallicities are limited to higher values.

Table 1. Occurrence Rates

Test	B&L $[\text{Fe}/\text{H}] > 0$	B&L $[\text{Fe}/\text{H}] \leq 0$	R21 $[\text{Fe}/\text{H}] > 0$	R21 $[\text{Fe}/\text{H}] \leq 0$	σ $[\text{Fe}/\text{H}] > 0$	σ $[\text{Fe}/\text{H}] \leq 0$
(1) Default	28.0 (+4.9 -4.6)%	4.5 (+2.6 -1.9)%	14.3 (+2.0 -1.8)%	5.0 (+1.6 -1.3)%	2.7σ	-0.2σ
(2) Close GG	19.2 (+4.3 -3.9)%	3.1 (+2.2 -1.5)%	9.5 (+1.7 -1.5)%	3.8 (+1.4 -1.1)%	2.3σ	-0.3σ
(3) Distant GG	18.3 (+4.4 -3.9)%	2.1 (+2.0 -1.2)%	7.4 (+1.5 -1.3)%	2.5 (+1.2 -0.9)%	2.7σ	-0.2σ
(4) Dynamically Hot	20.1 (+4.5 -4.0)%	2.0 (+1.9 -1.2)%	7.1 (+1.5 -1.3)%	1.6 (+1.0 -0.7)%	3.0σ	0.3σ
(5) Dynamically Cold	12.1 (+3.7 -3.2)%	3.2 (+2.3 -1.6)%	7.4 (+1.5 -1.3)%	2.9 (+1.2 -1.0)%	1.3σ	0.2σ
(6) Single GG	17.3 (+4.0 -3.6)%	4.1 (+2.4 -1.7)%	10.4 (+1.7 -1.5)%	3.1 (+1.2 -1.0)%	1.7σ	0.5σ
(7) Multi GG	8.0 (+3.0 -2.5)%	<2.0%	2.2 (+0.9 -0.7)%	0.7 (+0.7 -0.4)%	2.2σ	-0.3σ

NOTE—(1) Default: GG 1–10AU, 0.5–20M_{Jup}; (2) Close GG: 0.3–3AU, 0.5–20M_{Jup}; (3) Distant GG: 3–10AU, 0.5–20M_{Jup}; (4) Dynamically Hot: default GG with eccentricities >0.2 ; (5) Dynamically Cold: default GG with eccentricities <0.2 ; (6) Single GG: systems with a single gas giant in the default GG range; (7) Multi GG: systems with multiple gas giants in the default GG range. Median and 68% confidence intervals are quoted.

not exhibit any significant correlation for either dynamically hot or cold systems.

We next explore trends with gas giant multiplicity. Our sample has an average gas giant multiplicity of 1.3, while the R21 sample has an average multiplicity of 1.1. We break gas giant companions into single and multiple gas giant systems, where all gas giants considered fall in the default gas giant parameter space (1–10 AU, 0.5–20 M_{Jup}). Table 1 and Figure 4 show that for metal rich systems, the positive correlation gets slightly stronger when there are multiple gas giants (going from 1.7σ for single GG to 2.2σ for multi GG), whereas the correlation gets smaller and possibly becomes an anti-correlation

for metal-poor systems with multiple gas giants (going from 0.5σ for single GG systems to -0.3σ for multi-GG systems).

Finally, we constrain the inverse conditional probability linking super-Earths and gas giants. Namely, given a cold gas giant, what is the probability of finding an inner super-Earth $P(\text{SE}|GG)$? We can estimate this using the following:

$$P(\text{SE}|GG) = \frac{P(\text{GG}|\text{SE})P(\text{SE})}{P(\text{GG})}. \quad (2)$$

We take the calculated $P(\text{GG}|\text{SE})$ and $P(\text{GG})$ for metal-rich and metal-poor stars as shown in Table 1. For

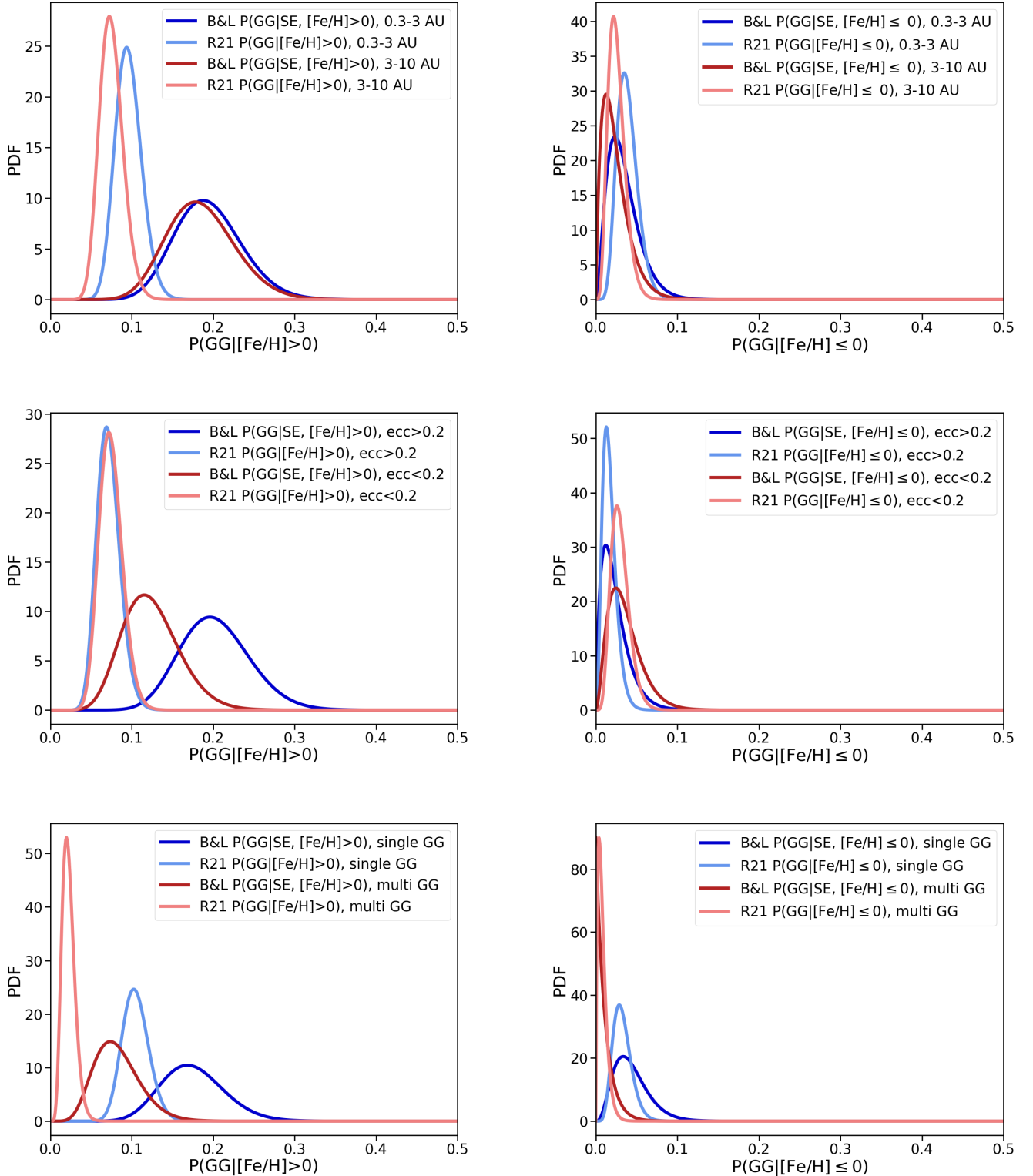


Figure 4. Comparison of conditional occurrence rates $P(\text{GG|SE})$ (labeled B&L) with field giant occurrence rates $P(\text{GG})$ (labeled R21) for metal-rich stars (left column) and metal-poor stars (right column). Top row: occurrence rates for close giants (0.3–3 AU) vs. distant giants (3–10 AU). Middle row: occurrence rates for dynamically hot giants ($e > 0.2$) vs. dynamically cold giants ($e < 0.2$). Bottom row: occurrence rates for systems of single giants vs. multiple giants. In general, the GG/SE correlation enhances in systems with distant, eccentric, and/or multiple giants around metal-rich stars. Giant multiplicity impacts the level of correlation around metal-poor stars where we see a slight anti-correlation.

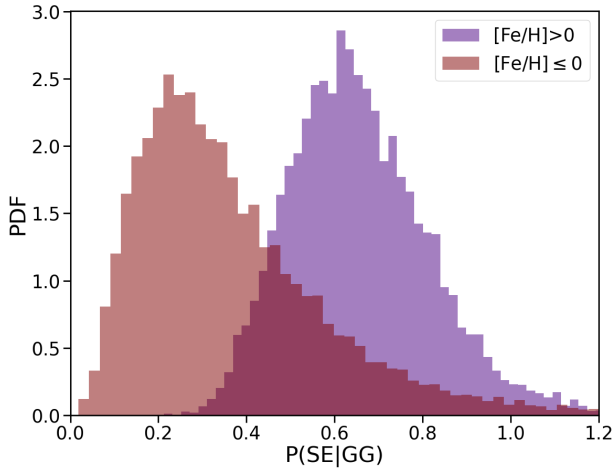


Figure 5. Comparing the inverse probability of super-Earths in systems hosting cold gas giants $P(\text{SE}|\text{GG})$ in metal-rich (maroon) and metal-poor (purple) systems. We find that while more than half of stars with $[\text{Fe}/\text{H}]>0$ hosting cold gas giants should also host a super-Earth, metal poor stars with gas giants may be less likely to host an inner super-Earth than other stars ($P(\text{SE})>P(\text{SE}|\text{GG}, [\text{Fe}/\text{H}]\leq 0)$).

$P(\text{SE})$ we take $P(\text{SE}) = 30 \pm 3\%$ from Zhu et al. (2018). Around metal-rich stars, $P(\text{SE}|\text{GG}, [\text{Fe}/\text{H}]>0) = 61.2 (+18.4 -12.7)\%$, and for their metal-poor counterparts, $P(\text{SE}|\text{GG}, [\text{Fe}/\text{H}]\leq 0) = 21.6 (+26.3 -8.7)\%$ (Figure 5). While more than half of metal rich stars hosting cold Jupiters should also host super-Earths, metal poor stars with gas giants might be less likely to host an inner super-Earth than other stars ($P(\text{SE})>P(\text{SE}|\text{GG}, [\text{Fe}/\text{H}]\leq 0)$).

7. DISCUSSION AND CONCLUSION

Using the largest sample size of systems to-date with both inner super-Earths and outer gas giants, we verify the positive correlation between the two populations that were previously reported by Zhu & Wu (2018) and Bryan et al. (2019). In particular, our results demonstrate that the correlation is particularly strong for metal-rich ($[\text{Fe}/\text{H}] > 0$) systems with no statistically significant correlation around metal-poor ($[\text{Fe}/\text{H}] \leq 0$) stars, verifying the argument of Zhu (2023) and highlighting the importance of system metallicity in shaping planetary architecture.

By combining the theory of core coagulation by pebble accretion and the observations of dust masses in Class 0/I disks, Chachan & Lee (2023) showed that the positive GG/SE correlation is naturally expected because disks that are massive enough to nucleate an outer planet will have enough mass to also create the inner planets, a consequence of low planet formation efficiency

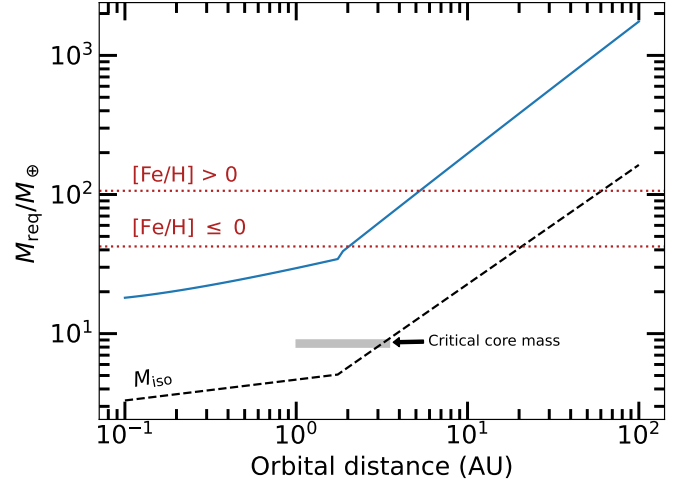


Figure 6. The required dust mass (M_{req} ; blue solid line) to create the pebble isolation mass (black dashed line) at each orbital distance following the calculation of Chachan & Lee (2023) adopting $1 M_{\odot}$ host star, $\alpha = 10^{-3}$, $\dot{M} = 10^{-8} M_{\odot} \text{ yr}^{-1}$, and the fragmentation velocity of 50 m s^{-1} from Kimura et al. (2020). The total disk mass for metal-poor system ($[\text{Fe}/\text{H}] \leq 0$) and metal-rich system ($[\text{Fe}/\text{H}] > 0$) are annotated with red dotted lines. The former value is taken as the median initial disk dust mass $42.33 M_{\oplus}$ for $0.6 - 1.4 M_{\odot}$ host stars (see Chachan & Lee 2023, their Figure 4) while the latter value is evaluated by multiplying $42.33 M_{\oplus}$ by $10^{0.4}$. Planetary cores of M_{iso} can nucleate in regions where the total disk dust mass is larger than M_{req} so that the spatial extent to which disk can generate planetary cores enlarges in metal-rich systems. Under this setup, M_{iso} core exceeds the critical core mass (gray box; Savignac & Lee 2023) and so is expected to trigger runaway gas accretion and become a giant at $\gtrsim 3$ AU.

at large orbital separations (see also Lin et al. 2018; Chachan et al. 2022). Furthermore, the inner cores will coagulate before all the filtered solids drift in towards the inner edge of the protoplanetary disk (see Chachan & Lee 2023, their Figure 5, bottom panel).²

In Figure 6, we illustrate the decisive role system metallicity—which we trace with the total initial disk dust mass—plays in establishing inner-outer planet correlation. We reproduce the required dust mass M_{req} to coagulate a planetary core of pebble isolation mass M_{iso} at each orbital distance as outlined in Chachan & Lee (2023) for $1 M_{\odot}$ host star, turbulent $\alpha = 10^{-3}$ and disk gas accretion rate $10^{-8} M_{\odot} \text{ yr}^{-1}$. We further

² The coagulation timescale being shorter than the drift time arises from the consideration of the material strength of silicate and icy grains being identical, consistent with modern lab measurements (e.g., Musiolik & Wurm 2019; Kimura et al. 2020) and the “No Snow Line” model of Mulders et al. (2021).

adopt grain fragmentation velocity of 50 m/s following Kimura et al. (2020, their Figure 13; the result also holds for lower fragmentation velocities used in the original work of Chachan & Lee (2023)). Comparing with the critical core mass to trigger runaway gas accretion computed in Savignac & Lee (2023) over 1–3.5 AU (under dusty gas accretion), we find that the outer planetary cores will likely nucleate gas giants beyond ~ 3 AU. Furthermore, and most importantly, with higher metallicity (i.e., larger solid reservoir), the spatial extent over which the disk can generate planetary cores enlarges, especially towards wider orbital separations where larger isolation mass and lower planet formation efficiency enforce larger required dust mass. This larger zone of core coagulation and the creation of giant-nucleating massive cores beyond ~ 3 AU around higher metallicity systems therefore explains concurrently the positive correlation between inner super-Earths and outer giants around stars of $[Fe/H] > 0$ and the slight enhancement of this correlation for giants that are farther away. The existence of giants at closer-in distances and their similarly positive correlation with the inner planets around metal-rich stars could be explained by a variation in the critical core mass owing to different opacity sources (see, e.g., Piso et al. 2015; Savignac & Lee 2023).

In the present paper, we find a slight difference in the strength of inner-outer correlation for systems with single vs. multiple outer giants, weakly favoring the latter. We can see in Figure 6 that at ~ 3 AU, to create $\sim 10M_{\oplus}$ core, the total dust mass in the disk needs to be $\sim 100M_{\oplus}$ and that the inner cores can be created as long as ~ 20 – $30M_{\oplus}$ worth of dust can be filtered through. Given the average outer giant multiplicity ~ 1.1 – 1.3 , the number of outer giants is likely at most 2 and so there

will be more than enough dust that will drift to the inner region, consistent with the similar level of inner-outer correlation with respect to outer giant multiplicity. In low metallicity systems however, the total mass budget would be quickly depleted with the formation of multiple cores which is in line with the observed anti-correlation around $[Fe/H] \leq 0$ stars.

An intriguing result from our analysis is the strong inner-outer correlation for gas giants with high eccentricity ($e > 0.2$). While the observed affinity for super-Earth systems to be neighbored by eccentric outer giant(s) could be a reflection of the tendency for metal-rich systems to harbor eccentric giants (see, e.g., Dawson & Murray-Clay 2013, for Jupiters inside 1 AU), we do not see the latter tendency in our sample, nor in R21 sample, which suggests that the metallicity-eccentricity relation is confined to warm and hot Jupiters. It may be that the more eccentric outer Jupiter aids the formation of inner super-Earths by facilitating core coagulation via orbital instabilities and merger events. Such a hypothesis will be a subject of Paper II where we will explore how the properties of the inner planets (e.g., radius, mass, multiplicity, eccentricities/inclinations, and the innermost orbital period) vary in systems with and without outer giants.

We thank Eugene Chiang, Heather Knutson, Yanqin Wu, Wei Zhu, and the referee for helpful conversations and feedback. M.L.B. acknowledges support by NSERC, the Heising-Simons Foundation, and by the Connaught New Researcher Award from the University of Toronto. E.J.L. gratefully acknowledges support by NSERC, by FRQNT, by the Trottier Space Institute, and by the William Dawson Scholarship from McGill University.

APPENDIX

A. FULL SAMPLE LIST AND AVERAGE SENSITIVITIES

Table A.1. Sample of systems

Target	M _★ (M _⊙)	[Fe/H]	N _{pl}	Disc.	Method	N _{obs}	Baseline (yrs)	GG Companion	Ref.
CoRoT-24	0.91±0.09	0.30±0.15	2	Transit		71	3.2	No	1
EPIC 220674823	0.95 (+0.06 -0.05)	0.11±0.05	2	Transit		101	3.4	No	2
EPIC 229004835	0.97±0.04	-0.12±0.05	1	Transit		126	2.3	No	2
EPIC 249893012	1.05±0.05	0.20±0.05	3	Transit		99	1.4	No	3
GJ 143	0.73±0.07	0.00±0.06	2	Transit		112	15.2	No	4
GJ 9827	0.61±0.01	-0.26±0.09	3	Transit		128	10.8	No	2
HD 137496	1.04±0.02	-0.03±0.04	2	Transit		172	2.5	Yes	5

Table A.1 *continued*

Table A.1 (*continued*)

Target	M_* (M_\odot)	[Fe/H]	N_{pl}	Disc.	Method	N_{obs}	Baseline (yrs)	GG Companion	Ref.
HD 15337	0.90±0.03	0.15±0.10	2	Transit		87	13.7	No	6 ¹
HD 183579	1.03±0.05	-0.07±0.09	1	Transit		56	7.9	No	7
HD 18599	0.86±0.02	0±0.10	1	Transit		103	4.8	No	8
HD 191939	0.81±0.04	-0.15±0.06	6	Transit		182	1.3	Yes	9 ²
HD 207897	0.80±0.04	-0.04±0.04	1	Transit		122	17.7	No	11
HD 213885	1.07±0.02	-0.04±0.03	2	Transit		238	10.2	No	46
HD 23472	0.67±0.03	-0.20±0.05	5	Transit		104	1.7	No	12
HD 307842	0.91±0.10	-0.13±0.08	1	Transit		58	2.1	No	13
HD 3167	0.84 (+0.05 -0.04)	0.04±0.05	4	Transit		452	5.3	No	2
HD 39091	1.07±0.04	0.09±0.04	3	Transit		402	2.2	Yes	45
HD 5278	1.13±0.04	-0.12±0.04	2	Transit		41	1.1	No	14
HD 73583	0.73±0.02	0±0.09	2	Transit		118	3.5	No	15
HD 80653	1.18±0.04	0.26±0.07	2	Transit		208	2.9	Yes	2
HD 86226	1.02±0.06	0.02 (+0.06 -0.04)	2	Transit		132	10.1	No	16
HIP 116454	0.76±0.03	-0.16±0.08	1	Transit		108	6.5	No	2
HIP 29442	0.89±0.04	0.24±0.05	3	Transit		83	2.5	No	85
HIP 9618	1.02 (+0.04 -0.08)	-0.08±0.10 ³	2	Transit		36	10.1	No	17
K2-100	1.15±0.05	0.22±0.09	1	Transit		78	1.3	No	39
K2-110	0.74±0.02	-0.34±0.03	1	Transit		32	4.0	No	2
K2-111	0.84±0.02	-0.46±0.05	2	Transit		161	4.4	No	2
K2-12	0.96 (+0.06 -0.05)	0±0.10	1	Transit		50	7.0	No	2
K2-131	0.80±0.03	-0.04±0.07	1	Transit		115	1.3	No	2
K2-136	0.74±0.04	-0.02±0.08	3	Transit		115	2.2	No	40
K2-141	0.71±0.03	0±0.10	2	Transit		83	4.1	No	2
K2-167	1.01 (+0.08 -0.07)	-0.40±0.06	1	Transit		82	6.1	No	2
K2-19	0.88±0.03	0.06±0.05	3	Transit		51	2.9	No	18
K2-199	0.71±0.02	-0.01±0.09	2	Transit		45	2.9	No	41
K2-216	0.70±0.03	0±0.10	1	Transit		30	1.3	No	19
K2-222	0.99±0.07	-0.32±0.06	1	Transit		70	4.4	No	2
K2-263	0.88±0.03	-0.08±0.05	1	Transit		95	4.2	No	2
K2-265	0.92±0.02	0.08±0.02	1	Transit		144	1.1	No	20
K2-32	0.83±0.02	-0.06±0.03	4	Transit		168	3.2	No	21
K2-36	0.79±0.01	-0.03±0.08	2	Transit		86	5.1	No	2
K2-38	1.05 (+0.07 -0.06)	0.24±0.07	2	Transit		83	3.4	No	2
K2-66	1.11±0.04	-0.05±0.02	1	Transit		38	1.3	No	22
KOI-142	0.99±0.02	0.27±0.06	3	Transit		47	9.0	Yes	92
KOI-351	1.11±0.03	0.08±0.03	8	Transit		34	11.2	Yes	92
KOI-94	1.28±0.05	0.02±0.01	4	Transit		70	7.3	No	92
Kepler-10	0.91±0.02	-0.15±0.04	3	Transit		291	11.0	No	2
Kepler-100	1.09±0.03	0.07 (+0.08 -0.05)	4	Transit		112	13.4	No	92
Kepler-101	1.17 (+0.07 -0.05)	0.33±0.07	2	Transit		40	1.2	No	42
Kepler-102	0.80±0.02	0.11±0.04	5	Transit		147	10.3	No	2
Kepler-103	1.21 (+0.02 -0.03)	0.16±0.04	2	Transit		60	4.4	No	2
Kepler-104	0.82±0.03	-0.38±0.10	3	Transit		44	11.3	No	92
Kepler-106	0.96±0.03	-0.12±0.11	4	Transit		48	9.8	No	92
Kepler-107	1.24±0.03	0.32±0.07	4	Transit		121	6.0	No	2
Kepler-109	1.09 (+0.09 -0.08)	-0.02±0.07	2	Transit		66	10.0	No	2
Kepler-11	0.99±0.03	0.07±0.10	6	Transit		31	11.6	No	92
Kepler-113	0.79±0.02	0.05±0.07	2	Transit		42	12.0	No	92
Kepler-126	1.11±0.03	-0.13±0.10	3	Transit		35	5.3	No	92
Kepler-129	1.24±0.04	0.29±0.10	3	Transit		35	7.8	Yes	92
Kepler-131	1.08±0.02	0.12±0.07	2	Transit		46	6.9	No	92
Kepler-139	1.08±0.03	0.27±0.10	4	Transit		38	11.8	Yes	92
Kepler-1655	1.03±0.04	-0.24±0.05	1	Transit		97	4.3	No	2

Table A.1 *continued*

Table A.1 (*continued*)

Target	M_\star (M_\odot)	[Fe/H]	N_{pl}	Disc.	Method	N_{obs}	Baseline (yrs)	GG Companion	Ref.
Kepler-1710	0.93±0.02	-0.07±0.10	1	Transit		21	12.2	No	92
Kepler-18	0.98±0.02	0.20±0.10	3	Transit		25	8.8	No	92
Kepler-19	0.90±0.02	-0.13±0.06	3	Transit		73	9.3	No	92
Kepler-20	0.93±0.05	0.07±0.08	6	Transit		161	10.1	No	2
Kepler-21	1.41 (+0.02 -0.03)	-0.03±0.10	1	Transit		98	5.4	No	2
Kepler-22	0.86 (+0.05 -0.04)	-0.26±0.07	1	Transit		71	10.7	No	2
Kepler-25	1.15±0.03	-0.04±0.10	3	Transit		99	11.3	No	92
Kepler-323	1.02±0.07	-0.14±0.05	2	Transit		48	6.1	No	2
Kepler-36	1.03±0.04	-0.18±0.04	2	Transit		25	9.2	No	92
Kepler-37	0.79±0.02	-0.36±0.05	4	Transit		108	12.4	No	92
Kepler-406	1.06±0.03	0.18±0.07	2	Transit		58	11.9	No	92
Kepler-407	1.10±0.03	0.33±0.07	2	Transit		98	11.0	Yes	92
Kepler-409	0.94±0.02	0.05±0.07	1	Transit		97	10.7	No	92
Kepler-454	1.03 (+0.04 -0.03)	0.32±0.08	3	Transit		147	12.1	Yes	2
Kepler-48	0.92±0.02	0.17±0.07	4	Transit		59	12.8	Yes	92
Kepler-50	1.15±0.04	-0.04±0.10	2	Transit		39	9.8	No	92
Kepler-507	1.14±0.03	0.16±0.10	1	Transit		49	10.8	No	92
Kepler-538	0.89 (+0.05 -0.04)	-0.09±0.07	1	Transit		111	9.1	No	2
Kepler-65	1.25±0.03	0.17±0.06	4	Transit		79	11.1	Yes	92
Kepler-68	1.06±0.02	0.11±0.06	4	Transit		225	12.4	Yes	2
Kepler-78	0.78 (+0.03 -0.05)	-0.18±0.08	1	Transit		201	6.3	No	2
Kepler-92	1.29±0.04	0.14±0.01	3	Transit		23	9.9	No	92
Kepler-93	0.91±0.03	-0.18±0.10	1	Transit		153	12.2	No	2
Kepler-94	0.82±0.02	0.34±0.07	2	Transit		39	12.0	Yes	92
Kepler-95	1.08±0.04	0.30±0.10	1	Transit		36	7.9	No	92
Kepler-96	1.01±0.02	0.04±0.07	1	Transit		55	10.9	No	92
Kepler-97	0.90±0.03	-0.20±0.07	1	Transit		31	8.0	No	92
Kepler-98	1.00±0.02	0.18±0.07	1	Transit		42	7.9	No	92
Kepler-99	0.82±0.02	0.18±0.07	1	Transit		45	7.0	No	92
TOI-1246	0.87±0.03	0.17±0.06	4	Transit		128	2.0	No	28
TOI-1416	0.80±0.04	0.08±0.05	2	Transit		205	2.2	No	29
TOI-1422	0.98 (+0.06 -0.07)	-0.09±0.07	2	Transit		112	1.6	No	30
TOI-1670	1.21±0.02	0.09±0.07	2	Transit		65	1.4	Yes	43
TOI-1736	1.08±0.04	0.14±0.01	2	Transit		152	2.6	Yes	81
TOI-1759	0.61±0.02	0.05±0.16	1	Transit		216	1.2	No	31
TOI-1807	0.76±0.03	-0.04±0.02	1	Transit		161	1.3	No	32
TOI-1853	0.84±0.04	0.11±0.08	1	Transit		56	1.5	No	82
TOI-2134	0.74±0.03	0.12±0.02	2	Transit		221	2.2	No	83
TOI-2141	0.94±0.02	-0.12±0.01	1	Transit		90	1.6	No	81
TOI-4010	0.88±0.03	0.37±0.07	4	Transit		112	1.5	Yes	33
TOI-431	0.78±0.07	0.20±0.05	3	Transit		200	15.8	No	34
TOI-500	0.74±0.02	0.12±0.08	4	Transit		197	1.0	No	35
TOI-5398	1.15±0.01	0.09±0.06	2	Transit		86	1.2	No	91
TOI-561	0.81±0.04	-0.40±0.05	4	Transit		316	2.9	No	36
TOI-969	0.73±0.01	0.18±0.02	2	Transit		94	1.3	Yes	37
WASP-132	0.78±0.03	0.18±0.12	2	Transit		36	2.0	No	44
WASP-47	1.04±0.03	0.38±0.05	4	Transit		246	9.4	Yes	38
Wolf 503	0.69±0.02	-0.47±0.08	1	Transit		115	3.1	No	2
55 Cnc	0.97±0.05	0.38±0.06	5	RV		1584	30.6	Yes	50
61 Vir	0.91±0.04	0.03±0.06	3	RV		954	28.9	No	50
BD-08 2823	0.74±0.07	-0.07±0.03	2	RV		83	5.0	No	78
BD-11 4672	0.65±0.03	-0.35±0.15	2	RV		111	14.2	Yes	68
DMPP-1	1.21±0.03	0.12±0.10	4	RV		148	2.1	No	48
DMPP-4	1.25±0.02	-0.01±0.06	1	RV		71	4.3	No	88

Table A.1 *continued*

Table A.1 (*continued*)

Target	M _★ (M _⊙)	[Fe/H]	N _{pl}	Disc.	Method	N _{obs}	Baseline (yrs)	GG Companion	Ref.
GJ 160.2	0.69±0.10 ⁴	-0.26±0.10 ³	1	RV		107	8.3	No	65
GJ 2056	0.62±0.08	-0.08±0.10 ³	2	RV		51	9.1	No	59
GJ 3942	0.63±0.07	-0.04±0.09	1	RV		145	3.3	No	58
GJ 414 A	0.69±0.01	0.24±0.07	2	RV		560	28.2	No	50
GJ 676 A	0.62±0.06	0.23±0.10	4	RV		127	8.9	Yes	49
GJ 9404	0.62±0.07	0.16±0.10	1	RV		54	3.9	No	87
HD 10180	1.06±0.05	0.08±0.01	6	RV		190	6.7	No	66
HD 102365	0.85±0.10 ⁴	-0.31±0.01	1	RV		149	12.5	No	72
HD 103949	0.77±0.04	-0.07±0.05	1	RV		48	8.2	No	61
HD 107148	1.11±0.04	0.30±0.06	2	RV		114	20.2	No	50
HD 109271	1.05±0.02	0.10±0.05	2	RV		100	7.5	No	74
HD 110067	0.80±0.04	-0.20±0.04	6	RV		111	1.9	No	90
HD 125595	0.76±0.02	0.02±0.06	1	RV		117	5.7	No	79
HD 125612	1.11±0.20	0.25±0.04	3	RV		72	12.1	Yes	69
HD 134060	1.09±0.10 ⁴	0.14±0.01	2	RV		339	13.2	No	53
HD 136352	0.87±0.04	-0.24±0.05	3	RV		458	19.3	No	52
HD 13808	0.77±0.02	-0.21±0.02	2	RV		246	11.1	No	64
HD 140901	0.99±0.12	0.09±0.01	2	RV		392	24.0	Yes	70
HD 141004	1.05±0.05	0.03±0.06	1	RV		1511	32.4	No	50
HD 1461	1.03±0.05	0.18±0.06	2	RV		1040	23.3	No	50
HD 154088	0.91±0.02	0.28±0.03	1	RV		187	11.4	No	51
HD 156668	0.77±0.02	0.05±0.06	2	RV		821	16.8	No	50
HD 158259	1.08±0.10	0±0.12	5	RV		290	7.1	No	47
HD 160691	1.13±0.02	0.28±0.03	4	RV		380	17.1	Yes	80
HD 164595	0.99±0.03	-0.04±0.08	1	RV		75	2.3	No	73
HD 164922	0.92±0.03	0.20±0.06	4	RV		742	23.1	No	50
HD 168009	0.99±0.04	0.02±0.06	1	RV		613	21.1	No	50
HD 175607	0.71±0.01	-0.62±0.01	1	RV		110	9.3	No	62
HD 176986	0.79±0.02	0.03±0.05	2	RV		259	13.2	No	55
HD 177565	1.0±0.10	0.08±0.01	1	RV		68	4.6	No	67
HD 181433	0.78±0.10 ⁴	0.33±0.13	3	RV		200	13.8	Yes	56
HD 189567	0.83±0.01	-0.24±0.01	2	RV		256	13.2	No	51
HD 190007	0.77±0.02	0.16±0.05	1	RV		191	21.3	No	63
HD 190360	0.99±0.04	0.23±0.06	2	RV		1243	23.5	Yes	50
HD 192310	0.84±0.03	0.08±0.06	2	RV		429	15.2	No	50
HD 20003	0.88±0.10 ⁴	0.04±0.02	2	RV		203	13.7	No	53
HD 204313	1.03±0.04	0.18±0.02	3	RV		193	14.2	Yes	75
HD 20781	0.70±0.10 ⁴	-0.11±0.02	4	RV		237	13.7	No	53
HD 211970	0.61±0.04	-0.50±0.10 ³	1	RV		52	8.5	No	61
HD 215497	0.92±0.05	0.23±0.07	2	RV		99	5.1	No	57
HD 216520	0.82±0.04	-0.16±0.10 ³	2	RV		804	18.7	No	63
HD 21693	0.80±0.10 ⁴	0±0.02	2	RV		213	11.3	No	53
HD 219134	0.79±0.03	0.08±0.06	5	RV		1176	27.1	No	50
HD 219828	1.23±0.10	0.19±0.03	2	RV		114	14.2	Yes	76
HD 22496	0.68±0.01	-0.08±0.02	1	RV		84	17.4	No	54
HD 24085	1.22±0.07	0.17±0.06	1	RV		25	8.7	No	61
HD 26965	0.78±0.08	-0.42±0.04	1	RV		1253	15.1	No	60
HD 31527	0.96±0.10 ⁴	-0.17±0.01	3	RV		268	13.9	No	53
HD 34445	1.11±0.06	0.14±0.06	6	RV		222	21.8	Yes	50
HD 39194	0.67±0.04	-0.61±0.02	3	RV		273	13.7	No	51
HD 39855	0.87±0.05	-0.46±0.10 ³	1	RV		25	6.2	No	61
HD 40307	0.77±0.05	-0.31±0.03	6	RV		226	10.4	No	49
HD 42618	0.92±0.05	-0.09±0.06	1	RV		835	23.4	No	50

Table A.1 *continued*

Table A.1 (*continued*)

Target	M_* (M_\odot)	[Fe/H]	N_{pl}	Disc.	Method	N_{obs}	Baseline (yrs)	GG Companion	Ref.
HD 4308	0.93±0.10	-0.35±0.01	1	RV		357	13.9	No	71
HD 45184	1.01±0.05	0.04±0.06	2	RV		339	23.4	No	50
HD 51608	0.80±0.10 ⁴	-0.07±0.01	2	RV		227	13.8	No	53
HD 64114	0.95±0.05	-0.03±0.10 ³	1	RV		28	7.2	No	61
HD 69830	0.89±0.04	0.01±0.06	3	RV		845	19.3	No	50
HD 77338	0.93±0.05	0.28±0.04	1	RV		32	7.2	No	77
HD 7924	0.80±0.03	-0.12±0.06	3	RV		1242	18.1	No	50
HD 90156	0.86±0.04	-0.18±0.06	1	RV		167	23.2	No	50
HD 93385	1.04±0.01	0.02±0.01	3	RV		241	13.2	No	51
HD 96700	0.89±0.01	-0.18±0.01	3	RV		254	14.4	No	51
HD 97658	0.77±0.03	-0.23±0.06	1	RV		785	22.0	No	50
HD 99492	0.85±0.03	0.29±0.06	2	RV		197	23.1	No	50
HIP 107772	0.63±0.08	-0.66±0.10 ³	1	RV		49	9.2	No	59
HIP 35173	0.79±0.05	0.13±0.10 ³	1	RV		39	8.8	No	61
HIP 38594	0.61±0.02	-0.17±0.10 ³	2	RV		38	8.9	No	59
HIP 4845	0.62±0.04	-0.5±0.10 ³	1	RV		94	11.1	No	59

NOTE—References: (1) Alonso et al. (2014), (2) Bonomo et al. (2023), (3) Hidalgo et al. (2020), (4) Dragomir et al. (2019), (5) Azevedo Silva et al. (2022), (6) Gandolfi et al. (2019), (7) Gan et al. (2021), (8) Desidera et al. (2023), (9) Lubin et al. (2022), (10) Barros et al. (2023), (11) Heidari et al. (2022), (12) Barros et al. (2022), (13) Hua et al. (2023), (14) Sozzetti et al. (2021), (15) Barragán et al. (2022), (16) Teske et al. (2020), (17) Osborn et al. (2023), (18) Petigura et al. (2020), (19) Persson et al. (2018), (20) Lam et al. (2018), (21) Lillo-Box et al. (2020), (22) Sinukoff et al. (2017), (23) Weiss et al. (2020), (24) Weiss et al. (2013), (25) Marcy et al. (2014), (26) Zhang et al. (2021), (27) Mills et al. (2019), (28) Turtelboom et al. (2022), (29) Deeg et al. (2023), (30) Naponiello et al. (2022), (31) Martioli et al. (2022), (32) Nardiello et al. (2022), (33) Kunimoto et al. (2023), (34) Osborn et al. (2021), (35) Serrano et al. (2022), (36) Brinkman et al. (2023), (37) Lillo-Box et al. (2023), (38) Bryant & Bayliss (2022), (39) Barragán et al. (2019), (40) Mayo et al. (2023), (41) Akana Murphy et al. (2021), (42) Bonomo et al. (2014), (43) Tran et al. (2022), (44) Hellier et al. (2017), (45) Hatzes et al. (2022), (46) Espinoza et al. (2020), (47) Hara et al. (2020), (48) Staab et al. (2020), (49) Bryan et al. (2019), (50) Rosenthal et al. (2021), (51) Unger et al. (2021), (52) Kane et al. (2020), (53) Udry et al. (2019), (54) Lillo-Box et al. (2021), (55) Suárez Mascareño et al. (2018), (56) Horner et al. (2019), (57) Lo Curto et al. (2010), (58) Perger et al. (2017), (59) Feng et al. (2020), (60) Ma et al. (2018), (61) Feng et al. (2019), (62) Mortier et al. (2016), (63) Burt et al. (2021), (64) Ahren et al. (2021), (65) Tuomi et al. (2014), (66) Lovis et al. (2011), (67) Feng et al. (2017), (68) Barbato et al. (2020), (69) Ment et al. (2018), (70) Feng et al. (2022), (71) Trifonov et al. (2020), (72) Tinney et al. (2011), (73) Courcol et al. (2015), (74) Lo Curto et al. (2013), (75) Díaz et al. (2016), (76) Santos et al. (2016), (77) Jenkins et al. (2013), (78) Hébrard et al. (2010), (79) Ségransan et al. (2011), (80) Benedict et al. (2022), (81) Martioli et al. (2023), (82) Naponiello et al. (2023), (83) Rescigno et al. (2024), (84) Osborne et al. (2024), (85) Damasso et al. (2023), (86) Dai et al. (2023), (87) Pinamonti et al. (2022), (88) Barnes et al. (2023), (89) Heidari et al. (2024), (90) Luque et al. (2023), (91) Mántovan et al. (2024), (92) Weiss et al. (2024)

¹ We note that Gandolfi et al. (2019) and Dumusque et al. (2019) independently reduced the same dataset and obtained the same time baseline, comparable uncertainties, and 87/85 data points. In subsequent analyses we use the dataset from Gandolfi et al. (2019).

² Orell-Miquel et al. (2023) publishes plots of additional datasets from CARMENES and HARPS-N but do not make them publicly available.

³ In the cases where uncertainties on stellar metallicities are not given, we assume an error of 0.1 dex.

⁴ In the cases where uncertainties on stellar mass are not given, we assume an error of 0.1 M_\odot .

Table A.2. Confirmed Gas Giants in Our Super-Earth System Sample

Target	GG Mass (M_{Jup})	GG Semi-major axis (AU)	M_* (M_\odot)	[Fe/H]
HD 137496 c	7.66±0.11	1.22±0.01	1.04±0.02	-0.03±0.04
HD 191939 f	6.5±4.5	4.8±2.2	0.81±0.04	-0.15±0.06
HD 39091 b	12.6±2.0	3.3±0.1	1.07±0.04	0.09±0.03
HD 80653 c	5.41 (+0.52 -0.44)	1.96±0.03	1.18±0.04	0.26±0.07
Kepler-129 d	6.34±0.14	3.26	1.24±0.04	0.29±0.10
Kepler-139 e	1.34±0.13	3.24	1.08±0.03	0.27±0.10
Kepler-407 c	11.09±0.05	3.27	1.07±0.03	0.33±0.07
Kepler-454 c	4.51±0.12	1.29±0.02	1.03 (+0.04 -0.03)	0.32±0.08

Table A.2 *continued*

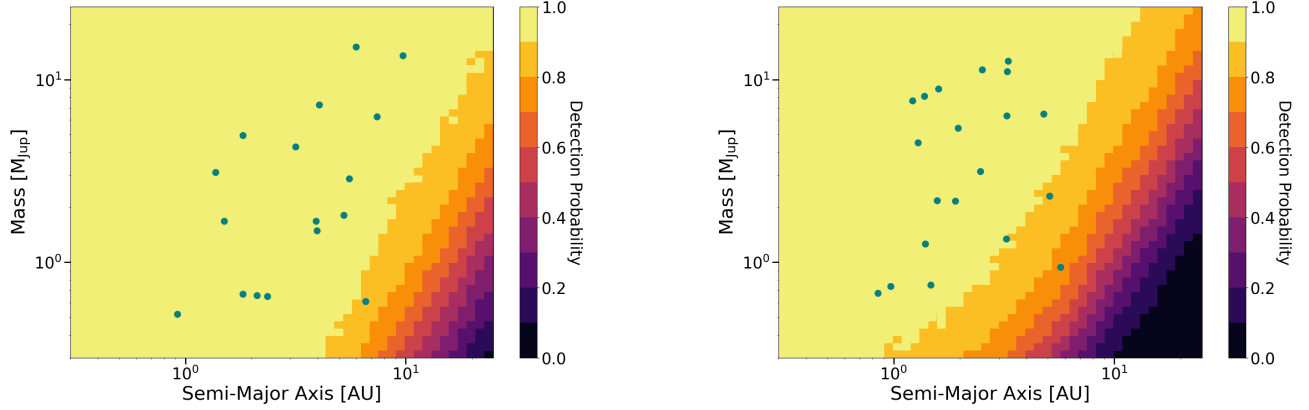


Figure A.1. Left: Average completeness map for the super-Earth RV sample with detected gas giants overplotted in teal. Right: Average completeness map for the super-Earth transit sample with detected gas giants overplotted in teal. Color scale represents detection probability. On average, the RV sample has higher completeness to distant gas giants typically driven by much longer time baselines and more data points. Accounting for differences in individual system sensitivity as well as these broad trends between transit and RV samples is key to calculating frequencies of gas giants in our sample of super-Earth systems.

Table A.2 (continued)

Target	GG Mass (M_{Jup})	GG Semi-major axis (AU)	M_\star (M_\odot)	[Fe/H]
Kepler-454 d	2.31 (+0.27 -0.16)	5.10 (+0.34 -0.19)	1.03 (+0.04 -0.03)	0.32±0.08
Kepler-48 e	2.16±0.06	1.90	0.92±0.02	0.17±0.07
Kepler-48 f	0.94±0.29	5.72	0.92±0.02	0.17±0.07
Kepler-65 e	0.68±0.07	0.85	1.25±0.03	0.17±0.06
Kepler-68 d	0.75±0.02	1.47±0.01	1.06±0.02	0.11±0.06
Kepler-94 c	8.89±0.12	1.60	0.82±0.02	0.34±0.07
KOI-142 c	0.65±0.02	0.15	0.99±0.02	0.27±0.06
KOI-142 d	3.15±0.17	2.47	0.99±0.02	0.27±0.06
KOI-351 h	0.74±0.11	0.97	1.11±0.03	0.08±0.03
TOI-1670 c	0.63 (+0.09 -0.08)	0.25±0.01	1.21±0.02	0.09±0.07
TOI-1736 c	8.09±0.20	1.38±0.02	1.08±0.04	0.14±0.01
TOI-4010 e	2.18 (+0.21 -0.20)	1.57 (+0.12 -0.13)	0.88±0.03	0.37±0.07
TOI-969 c	11.3 (+1.1 -0.9)	2.52 (+0.27 -0.29)	0.73±0.01	0.18±0.02
WASP-47 c	1.26±0.03	1.39±0.01	1.04±0.03	0.38±0.05
WASP-47 b	1.14±0.02	0.05±0.01	1.04±0.03	0.38±0.05
55 Cnc b	0.84±0.03	0.12±0.01	0.97±0.05	0.38±0.06
55 Cnc d	2.86±0.25	5.54±0.10	0.97±0.05	0.38±0.06
BD-11 4672 b	0.65 (+0.05 -0.06)	2.36±0.04	0.65±0.03	-0.35±0.15
GJ 676 A b	4.96±0.96	1.82±0.06	0.62±0.06	0.23±0.10
GJ 676 A c	13.5 (+1.0 -1.1)	9.73 (+0.63 -0.79)	0.62±0.06	0.23±0.1
HD 125612 b	3.1±0.4	1.37±0.08	1.11±0.20	0.25±0.04
HD 125612 d	7.28±0.93	4.06±0.25	1.11±0.20	0.25±0.04
HD 140901 c	6.28 (+1.34 -5.04)	7.42 (+0.32 -0.58)	0.99±0.12	0.09±0.01
HD 160691 b	1.68	1.50	1.13±0.02	0.28±0.03
HD 160691 c	1.81	5.24	1.13±0.02	0.28±0.03
HD 160691 e	0.52	0.92	1.13±0.02	0.28±0.03
HD 181433 c	0.67±0.01	1.82±0.01	0.78±0.10	0.33±0.13
HD 181433 d	0.61±0.01	6.60±0.22	0.78±0.10	0.33±0.13
HD 190360 b	1.49±0.04	3.96±0.05	0.99±0.04	0.23±0.06
HD 204313 b	4.28±0.30	3.17±0.12	1.03±0.04	0.18±0.02
HD 204313 d	1.68±0.30	3.93±0.14	1.03±0.04	0.18±0.02

Table A.2 continued

Table A.2 (*continued*)

Target	GG Mass (M_{Jup})	GG Semi-major axis (AU)	M_* (M_\odot)	[Fe/H]
HD 219828 c	15.10±0.85	5.96	1.23±0.10	0.19±0.03
HD 34445 b	0.66±0.04	2.11±0.04	1.11±0.06	0.14±0.06

REFERENCES

- Ahrer, E., Queloz, D., Rajpaul, V. M., et al. 2021, MNRAS, 503, 1248, doi: [10.1093/mnras/stab373](https://doi.org/10.1093/mnras/stab373)
- Akana Murphy, J. M., Kosiarek, M. R., Batalha, N. M., et al. 2021, AJ, 162, 294, doi: [10.3847/1538-3881/ac2830](https://doi.org/10.3847/1538-3881/ac2830)
- Alonso, R., Moutou, C., Endl, M., et al. 2014, A&A, 567, A112, doi: [10.1051/0004-6361/201118662](https://doi.org/10.1051/0004-6361/201118662)
- Azevedo Silva, T., Demangeon, O. D. S., Barros, S. C. C., et al. 2022, A&A, 657, A68, doi: [10.1051/0004-6361/202141520](https://doi.org/10.1051/0004-6361/202141520)
- Barbato, D., Pinamonti, M., Sozzetti, A., et al. 2020, A&A, 641, A68, doi: [10.1051/0004-6361/202037954](https://doi.org/10.1051/0004-6361/202037954)
- Barnes, J. R., Standing, M. R., Haswell, C. A., et al. 2023, MNRAS, 524, 5196, doi: [10.1093/mnras/stad2109](https://doi.org/10.1093/mnras/stad2109)
- Barragán, O., Aigrain, S., Kubyshkina, D., et al. 2019, MNRAS, 490, 698, doi: [10.1093/mnras/stz2569](https://doi.org/10.1093/mnras/stz2569)
- Barragán, O., Armstrong, D. J., Gandolfi, D., et al. 2022, MNRAS, 514, 1606, doi: [10.1093/mnras/stac638](https://doi.org/10.1093/mnras/stac638)
- Barros, S. C. C., Demangeon, O. D. S., Alibert, Y., et al. 2022, A&A, 665, A154, doi: [10.1051/0004-6361/202244293](https://doi.org/10.1051/0004-6361/202244293)
- Barros, S. C. C., Demangeon, O. D. S., Armstrong, D. J., et al. 2023, A&A, 673, A4, doi: [10.1051/0004-6361/202245741](https://doi.org/10.1051/0004-6361/202245741)
- Batygin, K., & Laughlin, G. 2015, Proceedings of the National Academy of Science, 112, 4214, doi: [10.1073/pnas.1423252112](https://doi.org/10.1073/pnas.1423252112)
- Benedict, G. F., McArthur, B. E., Nelan, E. P., et al. 2022, AJ, 163, 295, doi: [10.3847/1538-3881/ac6ac8](https://doi.org/10.3847/1538-3881/ac6ac8)
- Bonomo, A. S., Sozzetti, A., Lovis, C., et al. 2014, A&A, 572, A2, doi: [10.1051/0004-6361/201424617](https://doi.org/10.1051/0004-6361/201424617)
- Bonomo, A. S., Dumusque, X., Massa, A., et al. 2023, A&A, 677, A33, doi: [10.1051/0004-6361/202346211](https://doi.org/10.1051/0004-6361/202346211)
- Brinkman, C. L., Weiss, L. M., Dai, F., et al. 2023, AJ, 165, 88, doi: [10.3847/1538-3881/acad83](https://doi.org/10.3847/1538-3881/acad83)
- Bryan, M. L., Knutson, H. A., Lee, E. J., et al. 2019, AJ, 157, 52, doi: [10.3847/1538-3881/aaf57f](https://doi.org/10.3847/1538-3881/aaf57f)
- Bryant, E. M., & Bayliss, D. 2022, AJ, 163, 197, doi: [10.3847/1538-3881/ac58ff](https://doi.org/10.3847/1538-3881/ac58ff)
- Burt, J., Feng, F., Holden, B., et al. 2021, AJ, 161, 10, doi: [10.3847/1538-3881/abc2d0](https://doi.org/10.3847/1538-3881/abc2d0)
- Chachan, Y., & Lee, E. J. 2023, ApJL, 952, L20, doi: [10.3847/2041-8213/ace257](https://doi.org/10.3847/2041-8213/ace257)
- Chachan, Y., Dalba, P. A., Knutson, H. A., et al. 2022, ApJ, 926, 62, doi: [10.3847/1538-4357/ac3ed6](https://doi.org/10.3847/1538-4357/ac3ed6)
- Courcol, B., Bouchy, F., Pepe, F., et al. 2015, A&A, 581, A38, doi: [10.1051/0004-6361/201526329](https://doi.org/10.1051/0004-6361/201526329)
- Dai, F., Schlaufman, K. C., Reggiani, H., et al. 2023, AJ, 166, 49, doi: [10.3847/1538-3881/acdee8](https://doi.org/10.3847/1538-3881/acdee8)
- Damasso, M., Rodrigues, J., Castro-González, A., et al. 2023, A&A, 679, A33, doi: [10.1051/0004-6361/202347240](https://doi.org/10.1051/0004-6361/202347240)
- Dawson, R. I., & Murray-Clay, R. A. 2013, ApJL, 767, L24, doi: [10.1088/2041-8205/767/2/L24](https://doi.org/10.1088/2041-8205/767/2/L24)
- Deeg, H. J., Georgieva, I. Y., Nowak, G., et al. 2023, A&A, 677, A12, doi: [10.1051/0004-6361/202346370](https://doi.org/10.1051/0004-6361/202346370)
- Desidera, S., Damasso, M., Gratton, R., et al. 2023, A&A, 675, A158, doi: [10.1051/0004-6361/202244611](https://doi.org/10.1051/0004-6361/202244611)
- Díaz, R. F., Ségransan, D., Udry, S., et al. 2016, A&A, 585, A134, doi: [10.1051/0004-6361/201526729](https://doi.org/10.1051/0004-6361/201526729)
- Dragomir, D., Teske, J., Günther, M. N., et al. 2019, ApJL, 875, L7, doi: [10.3847/2041-8213/ab12ed](https://doi.org/10.3847/2041-8213/ab12ed)
- Dumusque, X., Turner, O., Dorn, C., et al. 2019, A&A, 627, A43, doi: [10.1051/0004-6361/201935457](https://doi.org/10.1051/0004-6361/201935457)
- Espinoza, N., Brahm, R., Henning, T., et al. 2020, MNRAS, 491, 2982, doi: [10.1093/mnras/stz3150](https://doi.org/10.1093/mnras/stz3150)
- Feng, F., Tuomi, M., & Jones, H. R. A. 2017, MNRAS, 470, 4794, doi: [10.1093/mnras/stx1126](https://doi.org/10.1093/mnras/stx1126)
- Feng, F., Crane, J. D., Xuesong Wang, S., et al. 2019, ApJS, 242, 25, doi: [10.3847/1538-4365/ab1b16](https://doi.org/10.3847/1538-4365/ab1b16)
- Feng, F., Shectman, S. A., Clement, M. S., et al. 2020, ApJS, 250, 29, doi: [10.3847/1538-4365/abb139](https://doi.org/10.3847/1538-4365/abb139)
- Feng, F., Butler, R. P., Vogt, S. S., et al. 2022, ApJS, 262, 21, doi: [10.3847/1538-4365/ac7e57](https://doi.org/10.3847/1538-4365/ac7e57)
- Gan, T., Bedell, M., Wang, S. X., et al. 2021, MNRAS, 507, 2220, doi: [10.1093/mnras/stab2224](https://doi.org/10.1093/mnras/stab2224)
- Gandolfi, D., Fossati, L., Livingston, J. H., et al. 2019, ApJL, 876, L24, doi: [10.3847/2041-8213/ab17d9](https://doi.org/10.3847/2041-8213/ab17d9)
- Hara, N. C., Bouchy, F., Stalport, M., et al. 2020, A&A, 636, L6, doi: [10.1051/0004-6361/201937254](https://doi.org/10.1051/0004-6361/201937254)
- Hatzes, A. P., Gandolfi, D., Korth, J., et al. 2022, AJ, 163, 223, doi: [10.3847/1538-3881/ac5dc9](https://doi.org/10.3847/1538-3881/ac5dc9)

- Hébrard, G., Udry, S., Lo Curto, G., et al. 2010, A&A, 512, A46, doi: [10.1051/0004-6361/200913525](https://doi.org/10.1051/0004-6361/200913525)
- Heidari, N., Boisse, I., Orell-Miquel, J., et al. 2022, A&A, 658, A176, doi: [10.1051/0004-6361/202141429](https://doi.org/10.1051/0004-6361/202141429)
- Heidari, N., Boisse, I., Hara, N. C., et al. 2024, A&A, 681, A55, doi: [10.1051/0004-6361/202347897](https://doi.org/10.1051/0004-6361/202347897)
- Hellier, C., Anderson, D. R., Collier Cameron, A., et al. 2017, MNRAS, 465, 3693, doi: [10.1093/mnras/stw3005](https://doi.org/10.1093/mnras/stw3005)
- Herman, M. K., Zhu, W., & Wu, Y. 2019, AJ, 157, 248, doi: [10.3847/1538-3881/ab1f70](https://doi.org/10.3847/1538-3881/ab1f70)
- Hidalgo, D., Pallé, E., Alonso, R., et al. 2020, A&A, 636, A89, doi: [10.1051/0004-6361/201937080](https://doi.org/10.1051/0004-6361/201937080)
- Horner, J., Wittenmyer, R. A., Wright, D. J., et al. 2019, AJ, 158, 100, doi: [10.3847/1538-3881/ab2e78](https://doi.org/10.3847/1538-3881/ab2e78)
- Hua, X., Wang, S. X., Teske, J. K., et al. 2023, AJ, 166, 32, doi: [10.3847/1538-3881/acd751](https://doi.org/10.3847/1538-3881/acd751)
- Jenkins, J. S., Jones, H. R. A., Tuomi, M., et al. 2013, ApJ, 766, 67, doi: [10.1088/0004-637X/766/2/67](https://doi.org/10.1088/0004-637X/766/2/67)
- Kane, S. R., Yalçınkaya, S., Osborn, H. P., et al. 2020, AJ, 160, 129, doi: [10.3847/1538-3881/aba835](https://doi.org/10.3847/1538-3881/aba835)
- Kimura, H., Wada, K., Kobayashi, H., et al. 2020, MNRAS, 498, 1801, doi: [10.1093/mnras/staa2467](https://doi.org/10.1093/mnras/staa2467)
- Kunimoto, M., Vanderburg, A., Huang, C. X., et al. 2023, AJ, 166, 7, doi: [10.3847/1538-3881/acd537](https://doi.org/10.3847/1538-3881/acd537)
- Lam, K. W. F., Santerne, A., Sousa, S. G., et al. 2018, A&A, 620, A77, doi: [10.1051/0004-6361/201834073](https://doi.org/10.1051/0004-6361/201834073)
- Lillo-Box, J., Lopez, T. A., Santerne, A., et al. 2020, A&A, 640, A48, doi: [10.1051/0004-6361/202037896](https://doi.org/10.1051/0004-6361/202037896)
- Lillo-Box, J., Faria, J. P., Suárez Mascareño, A., et al. 2021, A&A, 654, A60, doi: [10.1051/0004-6361/202141714](https://doi.org/10.1051/0004-6361/202141714)
- Lillo-Box, J., Gandolfi, D., Armstrong, D. J., et al. 2023, A&A, 669, A109, doi: [10.1051/0004-6361/202243879](https://doi.org/10.1051/0004-6361/202243879)
- Lin, J. W., Lee, E. J., & Chiang, E. 2018, MNRAS, 480, 4338, doi: [10.1093/mnras/sty2159](https://doi.org/10.1093/mnras/sty2159)
- Lo Curto, G., Mayor, M., Benz, W., et al. 2010, A&A, 512, A48, doi: [10.1051/0004-6361/200913523](https://doi.org/10.1051/0004-6361/200913523)
- . 2013, A&A, 551, A59, doi: [10.1051/0004-6361/201220415](https://doi.org/10.1051/0004-6361/201220415)
- Lovis, C., Ségransan, D., Mayor, M., et al. 2011, A&A, 528, A112, doi: [10.1051/0004-6361/201015577](https://doi.org/10.1051/0004-6361/201015577)
- Lubin, J., Van Zandt, J., Holcomb, R., et al. 2022, AJ, 163, 101, doi: [10.3847/1538-3881/ac3d38](https://doi.org/10.3847/1538-3881/ac3d38)
- Luque, R., Osborn, H. P., Leleu, A., et al. 2023, Nature, 623, 932, doi: [10.1038/s41586-023-06692-3](https://doi.org/10.1038/s41586-023-06692-3)
- Ma, B., Ge, J., Mutterspaugh, M., et al. 2018, MNRAS, 480, 2411, doi: [10.1093/mnras/sty1933](https://doi.org/10.1093/mnras/sty1933)
- Mantovan, G., Malavolta, L., Desidera, S., et al. 2024, A&A, 682, A129, doi: [10.1051/0004-6361/202347472](https://doi.org/10.1051/0004-6361/202347472)
- Marcy, G. W., Isaacson, H., Howard, A. W., et al. 2014, ApJS, 210, 20, doi: [10.1088/0067-0049/210/2/20](https://doi.org/10.1088/0067-0049/210/2/20)
- Martioli, E., Hébrard, G., Fouqué, P., et al. 2022, A&A, 660, A86, doi: [10.1051/0004-6361/202142540](https://doi.org/10.1051/0004-6361/202142540)
- Martioli, E., Hébrard, G., de Almeida, L., et al. 2023, A&A, 680, A84, doi: [10.1051/0004-6361/202347744](https://doi.org/10.1051/0004-6361/202347744)
- Mayo, A. W., Dressing, C. D., Vanderburg, A., et al. 2023, AJ, 165, 235, doi: [10.3847/1538-3881/acca1c](https://doi.org/10.3847/1538-3881/acca1c)
- Ment, K., Fischer, D. A., Bakos, G., Howard, A. W., & Isaacson, H. 2018, AJ, 156, 213, doi: [10.3847/1538-3881/aae1f5](https://doi.org/10.3847/1538-3881/aae1f5)
- Mills, S. M., Howard, A. W., Weiss, L. M., et al. 2019, AJ, 157, 145, doi: [10.3847/1538-3881/ab0899](https://doi.org/10.3847/1538-3881/ab0899)
- Morbidelli, A., Tsiganis, K., Crida, A., Levison, H. F., & Gomes, R. 2007, AJ, 134, 1790, doi: [10.1086/521705](https://doi.org/10.1086/521705)
- Mortier, A., Faria, J. P., Santos, N. C., et al. 2016, A&A, 585, A135, doi: [10.1051/0004-6361/201526905](https://doi.org/10.1051/0004-6361/201526905)
- Mulders, G. D., Drażkowska, J., van der Marel, N., Ciesla, F. J., & Pascucci, I. 2021, ApJL, 920, L1, doi: [10.3847/2041-8213/ac2947](https://doi.org/10.3847/2041-8213/ac2947)
- Musiolik, G., & Wurm, G. 2019, ApJ, 873, 58, doi: [10.3847/1538-4357/ab0428](https://doi.org/10.3847/1538-4357/ab0428)
- Naponiello, L., Mancini, L., Damasso, M., et al. 2022, A&A, 667, A8, doi: [10.1051/0004-6361/202244079](https://doi.org/10.1051/0004-6361/202244079)
- Naponiello, L., Mancini, L., Sozzetti, A., et al. 2023, Nature, 622, 255, doi: [10.1038/s41586-023-06499-2](https://doi.org/10.1038/s41586-023-06499-2)
- Nardiello, D., Malavolta, L., Desidera, S., et al. 2022, A&A, 664, A163, doi: [10.1051/0004-6361/202243743](https://doi.org/10.1051/0004-6361/202243743)
- Orell-Miquel, J., Nowak, G., Murgas, F., et al. 2023, A&A, 669, A40, doi: [10.1051/0004-6361/202244120](https://doi.org/10.1051/0004-6361/202244120)
- Osborn, A., Armstrong, D. J., Cale, B., et al. 2021, MNRAS, 507, 2782, doi: [10.1093/mnras/stab2313](https://doi.org/10.1093/mnras/stab2313)
- Osborn, H. P., Nowak, G., Hébrard, G., et al. 2023, MNRAS, 523, 3069, doi: [10.1093/mnras/stad1319](https://doi.org/10.1093/mnras/stad1319)
- Osborne, H. L. M., Van Eylen, V., Goffo, E., et al. 2024, MNRAS, 527, 11138, doi: [10.1093/mnras/stad3837](https://doi.org/10.1093/mnras/stad3837)
- Perger, M., Ribas, I., Damasso, M., et al. 2017, A&A, 608, A63, doi: [10.1051/0004-6361/201731307](https://doi.org/10.1051/0004-6361/201731307)
- Persson, C. M., Fridlund, M., Barragán, O., et al. 2018, A&A, 618, A33, doi: [10.1051/0004-6361/201832867](https://doi.org/10.1051/0004-6361/201832867)
- Petigura, E. A., Livingston, J., Batygin, K., et al. 2020, AJ, 159, 2, doi: [10.3847/1538-3881/ab5220](https://doi.org/10.3847/1538-3881/ab5220)
- Pinamonti, M., Sozzetti, A., Maldonado, J., et al. 2022, A&A, 664, A65, doi: [10.1051/0004-6361/202142828](https://doi.org/10.1051/0004-6361/202142828)
- Piso, A.-M. A., Youdin, A. N., & Murray-Clay, R. A. 2015, ApJ, 800, 82, doi: [10.1088/0004-637X/800/2/82](https://doi.org/10.1088/0004-637X/800/2/82)
- Rescigno, F., Hébrard, G., Vanderburg, A., et al. 2024, MNRAS, 527, 5385, doi: [10.1093/mnras/stad3255](https://doi.org/10.1093/mnras/stad3255)
- Rosenthal, L. J., Fulton, B. J., Hirsch, L. A., et al. 2021, ApJS, 255, 8, doi: [10.3847/1538-4365/abe23c](https://doi.org/10.3847/1538-4365/abe23c)
- Rosenthal, L. J., Knutson, H. A., Chachan, Y., et al. 2022, ApJS, 262, 1, doi: [10.3847/1538-4365/ac7230](https://doi.org/10.3847/1538-4365/ac7230)

- Santos, N. C., Santerne, A., Faria, J. P., et al. 2016, *A&A*, 592, A13, doi: [10.1051/0004-6361/201628374](https://doi.org/10.1051/0004-6361/201628374)
- Savignac, V., & Lee, E. J. 2023, arXiv e-prints, arXiv:2310.06013, doi: [10.48550/arXiv.2310.06013](https://doi.org/10.48550/arXiv.2310.06013)
- Ségransan, D., Mayor, M., Udry, S., et al. 2011, *A&A*, 535, A54, doi: [10.1051/0004-6361/200913580](https://doi.org/10.1051/0004-6361/200913580)
- Serrano, L. M., Gandolfi, D., Mustill, A. J., et al. 2022, *Nature Astronomy*, 6, 736, doi: [10.1038/s41550-022-01641-y](https://doi.org/10.1038/s41550-022-01641-y)
- Sinukoff, E., Howard, A. W., Petigura, E. A., et al. 2017, *AJ*, 153, 271, doi: [10.3847/1538-3881/aa725f](https://doi.org/10.3847/1538-3881/aa725f)
- Sozzetti, A., Damasso, M., Bonomo, A. S., et al. 2021, *A&A*, 648, A75, doi: [10.1051/0004-6361/202040034](https://doi.org/10.1051/0004-6361/202040034)
- Staab, D., Haswell, C. A., Barnes, J. R., et al. 2020, *Nature Astronomy*, 4, 399, doi: [10.1038/s41550-019-0974-x](https://doi.org/10.1038/s41550-019-0974-x)
- Suárez Mascareño, A., González Hernández, J. I., Rebolo, R., et al. 2018, *A&A*, 612, A41, doi: [10.1051/0004-6361/201732042](https://doi.org/10.1051/0004-6361/201732042)
- Teske, J., Díaz, M. R., Luque, R., et al. 2020, *AJ*, 160, 96, doi: [10.3847/1538-3881/ab9f95](https://doi.org/10.3847/1538-3881/ab9f95)
- Tinney, C. G., Butler, R. P., Jones, H. R. A., et al. 2011, *ApJ*, 727, 103, doi: [10.1088/0004-637X/727/2/103](https://doi.org/10.1088/0004-637X/727/2/103)
- Tran, Q. H., Bowler, B. P., Endl, M., et al. 2022, *AJ*, 163, 225, doi: [10.3847/1538-3881/ac5c4f](https://doi.org/10.3847/1538-3881/ac5c4f)
- Trifonov, T., Tal-Or, L., Zechmeister, M., et al. 2020, *A&A*, 636, A74, doi: [10.1051/0004-6361/201936686](https://doi.org/10.1051/0004-6361/201936686)
- Tuomi, M., Jones, H. R. A., Barnes, J. R., Anglada-Escudé, G., & Jenkins, J. S. 2014, *MNRAS*, 441, 1545, doi: [10.1093/mnras/stu358](https://doi.org/10.1093/mnras/stu358)
- Turtelboom, E. V., Weiss, L. M., Dressing, C. D., et al. 2022, *AJ*, 163, 293, doi: [10.3847/1538-3881/ac69e5](https://doi.org/10.3847/1538-3881/ac69e5)
- Udry, S., Dumusque, X., Lovis, C., et al. 2019, *A&A*, 622, A37, doi: [10.1051/0004-6361/201731173](https://doi.org/10.1051/0004-6361/201731173)
- Unger, N., Ségransan, D., Queloz, D., et al. 2021, *A&A*, 654, A104, doi: [10.1051/0004-6361/202141351](https://doi.org/10.1051/0004-6361/202141351)
- Walsh, K. J., Morbidelli, A., Raymond, S. N., O'Brien, D. P., & Mandell, A. M. 2011, *Nature*, 475, 206, doi: [10.1038/nature10201](https://doi.org/10.1038/nature10201)
- Weiss, L. M., Marcy, G. W., Rowe, J. F., et al. 2013, *ApJ*, 768, 14, doi: [10.1088/0004-637X/768/1/14](https://doi.org/10.1088/0004-637X/768/1/14)
- Weiss, L. M., Fabrycky, D. C., Agol, E., et al. 2020, *AJ*, 159, 242, doi: [10.3847/1538-3881/ab88ca](https://doi.org/10.3847/1538-3881/ab88ca)
- Weiss, L. M., Isaacson, H., Howard, A. W., et al. 2024, *ApJS*, 270, 8, doi: [10.3847/1538-4365/ad0cab](https://doi.org/10.3847/1538-4365/ad0cab)
- Wittenmyer, R. A., Wang, S., Horner, J., et al. 2020, *MNRAS*, 492, 377, doi: [10.1093/mnras/stz3436](https://doi.org/10.1093/mnras/stz3436)
- Zhang, J., Weiss, L. M., Huber, D., et al. 2021, *AJ*, 162, 89, doi: [10.3847/1538-3881/ac0634](https://doi.org/10.3847/1538-3881/ac0634)
- Zhu, W. 2023, arXiv e-prints, arXiv:2306.16691, doi: [10.48550/arXiv.2306.16691](https://doi.org/10.48550/arXiv.2306.16691)
- Zhu, W., Petrovich, C., Wu, Y., Dong, S., & Xie, J. 2018, *ApJ*, 860, 101, doi: [10.3847/1538-4357/aac6d5](https://doi.org/10.3847/1538-4357/aac6d5)
- Zhu, W., & Wu, Y. 2018, *AJ*, 156, 92, doi: [10.3847/1538-3881/aad22a](https://doi.org/10.3847/1538-3881/aad22a)